PAPER

View Article Online
View Journal | View Issue

Synthesis of a bistriazolyl-phenanthroline–Cu(II) complex immobilized on nanomagnetic iron oxide as a novel green catalyst for synthesis of imidazoles *via* annulation reactions†

Raed H. Althomali,[a] Ebraheem Abdu Musad Saleh, *[a] Riyadh Hasan Mohammed Ali,[b] Ikromjon Ilkhomidinovich Mamadoliev,[cd] Montather F. Ramadan,[e] Ashwaq Talib Kareem,[f] Saurabh Aggarwal[g] and Salema K. Hadrawi[h]

We designed and prepared a novel *N*-heterocycle-based nanocatalyst by a post synthetic method, namely the [Fe_3O_4@DAA-BTrzPhen–Cu(II)] composite. In this method, bistriazolyl-phenanthroline groups were stepwise synthesized on an Fe_3O_4 substrate and used as a tetradentate nitrogenous ligand for coordinating to copper ions. The obtained nanocomposite was well characterized using FT-IR, PXRD, TGA, EDAX, ICP-OES, EDX-mapping, SEM, TEM, VSM and BET analyses, which confirm the formation of a thermostable crystalline spherical particle morphology with the particle size in the range of 17 nm to 25 nm and a magnetization value of 42 emu g^{-1}. Also, the catalytic activity of [Fe_3O_4@DAA-BTrzPhen–Cu(II)] as a novel and magnetically separable heterogeneous nanocatalyst was evaluated in preparing various tetrasubstituted imidazole derivatives from one-pot four-component condensation of anilines, aldehydes, 1,2-diketones and ammonium acetate, and favorable products were produced with excellent yields. The stability, low Cu leaching, and heterogenous nature of the nanocatalyst were confirmed by hot-filtration and leaching tests. The copper based nanocatalyst could be easily recovered by magnetic field separation and recycled at least 8 times in a row without noticeable loss in its catalytic activity.

1. Introduction

Designing new heterogeneous catalytic processes is crucial in chemical engineering and catalysis.[1] Heterogeneous catalysis plays a pivotal role in various industrial applications such as petroleum refining, pharmaceutical synthesis, and environmental protection.[2] The primary goal of process design is to develop highly efficient catalysts for selective and sustainable reactions, improving rates and minimizing by-products.[3–5] Diligent researchers work on identifying novel catalyst materials and exploring innovative synthesis techniques.[6] By harnessing the potential of heterogeneous catalysis, scientists contribute to cleaner, greener, and more resource-efficient chemical processes, building a sustainable and eco-friendly future.[7,8]

Magnetic catalysts enable straightforward recovery and reusability with minimal reduction in their magnetic properties, setting them apart from traditional homogeneous catalysts.[9–12] In this sense, the extraordinary significance of Fe_3O_4 magnetic nanoparticles in catalysis science is unquestionable.[13,14] Their attributes, including high stability, low toxicity, and an impressive surface area, make them an excellent choice for reusable materials in organic compound synthesis.[15,16] Researchers have ingeniously coated the surface of these magnetic nanoparticles with diverse molecules, unlocking their potential in effective catalytic processes and driving significant advancements in chemical research.[17,18] The increasing focus on green chemistry aims to replace costly, hazardous, and polluting catalysts with environmentally friendly and highly stable heterogeneous catalysts.[19]

Cu-based catalysts are crucial in multicomponent reactions in organic chemistry, combining three or more reactants to produce complex molecules efficiently.[20,21] Demonstrating high efficiency and selectivity, these catalysts streamline synthesis,

[a] Department of Chemistry, College of Arts and Science, Prince Sattam Bin Abdulaziz University, Wadi Al-Dawasir 11991, Saudi Arabia. E-mail: eabdumusadsaleh@gmail.com

[b] Department of Medical Laboratory, Al-Rafidain University College, Iraq, Baghdad

[c] Department of Medical Chemistry, Samarkand State Medical Institute, Samarkand, Uzbekistan

[d] Department of Anatomy, Tashkent State Dental Institute, Tashkent, Uzbekistan

[e] College of Dentistry, Al-Ayen University, Thi-Qar, Iraq

[f] College of Pharmacy, National University of Science and Technology, Dhi Qar, Iraq

[g] Department of Mechanical Engineering, Uttaranchal Institute of Technology, Uttaranchal University, Dehradun-248007, India

[h] Refrigeration and Air-conditioning Technical Engineering Department, College of Technical Engineering, The Islamic University, Najaf, Iraq

† Electronic supplementary information (ESI) available. See DOI: https://doi.org/10.1039/d3na00653k

saving time and resources.[22,23] Cu-complexes play a crucial role in enabling multicomponent reactions, offering versatility and enhancing the range of synthesized compounds.[24,25] Their significance drives advancements in organic chemistry, leading to the discovery of novel pharmaceuticals, agrochemicals, and functional materials.[26]

The phenanthroline ligand consists of three fused benzene rings and two nitrogen atoms in positions 1 and 10.[27] On the other hand, triazoles are a class of five-membered ring heterocyclic compounds containing three nitrogen and two carbon atoms. They have different isomers, such as 1,2,3-triazole and 1,2,4-triazole, each having distinct properties and applications.[28] Both of these compounds and their derivatives have separately been widely used as ligands in coordination chemistry due to their ability to form stable complexes with metal ions and fantastic properties.[27,29] This information encourages us to develop a novel ligand containing both of these heterocycles in its structure with an engineered position of functional groups for metal complexation as well as easy immobilization capacity. For this purpose, in this work a bistriazolylphenanthroline compound was designed as the target ligand that was formed by connecting two triazole moieties to a phenanthroline. At each end of this molecule an amino acid chain was placed that was utilized for grafting on an Fe_3O_4 solid support and successful heterogenization of the target catalytic complex. Based on the good coordination characteristics of copper, it was selected as the metal center of our catalytic complex, and its application was employed in the synthesis of annulated N-heterocycles.

Multicomponent reactions (MCRs) represent a potent and efficient approach in synthetic chemistry, enabling the rapid assembly of complex molecules by combining multiple reactants in a single step.[30–32] These reactions have earned widespread recognition in the field of organic synthesis due to their ability to streamline processes, minimize waste, and enhance overall yield. MCRs offer a versatile toolkit for creating diverse molecular structures, making them essential in developing innovative compounds applicable across various domains, from drug discovery to materials science.[30,33–36]

Highly substituted imidazoles are heterocyclic compounds that contain nitrogen atoms in their ring structures.[37,38] These molecules have diverse structures with various functional groups, making them ideal substrates for testing the catalytic performance of new catalysts.[39] The synthesis of these compounds allows researchers to evaluate the catalyst's efficiency and selectivity in different types of reactions, such as condensation, cyclization, or hydrogenation,[40–42] and provides a robust platform for examining the catalytic performance of new catalysts.[43] Their diverse structures and application in pharmaceutical and material synthesis make them important tools in catalysis research and development.[44,45]

In our study, we synthesized a novel Cu-based bistriazolylphenanthroline complex by connecting two triazole moieties to a phenanthroline backbone. This complex was immobilized onto the surface of a nano-magnetic Fe_3O_4 support, through amino acid functionalities located at its ends. This design choice incorporates four electron-donating nitrogen atoms within the ligand structure. The presence of these nitrogen atoms, in conjunction with resonance effects and the formation of a stable π-system, facilitates the robust coordination of this nitrogen-rich ligand with copper ions, resulting in the formation of a stable catalytic complex. This resulting catalyst was effectively utilized in the synthesis of annulated N-heterocycles including highly substituted imidazoles, showcasing its potential for diverse applications in chemical transformations.

2. Experimental

2.1. Materials and methods

2.1.1. Chemicals and reagents. All chemicals and solvents utilized in this investigation adhered to rigorous analytical grade standards and were sourced from reputable suppliers, specifically Merck Company (Germany) and Sigma Aldrich (USA).

2.1.2. Instrumentation. Our research was underpinned by a comprehensive suite of advanced instruments, enabling meticulous characterization and analysis: to identify functional groups present on the catalyst surface, we employed a PerkinElmer Fourier Transform Infrared (FTIR) spectrometer (USA) operating within the range of 400–4000 cm^{-1}. To delineate the crystallography of nanoparticles, we conducted X-ray diffraction (XRD) analysis using a Bruker XRD instrument (Germany), covering 2θ angles ranging from 20° to 80° and employing a copper radiation source ($\lambda = 1.5405$ Å). Materials underwent Thermogravimetric Analysis (TGA) in a BAHR STA503 instrument (Germany) spanning a temperature range of 30 °C to 800 °C, with a heating rate of 10 °C min^{-1} and an argon flow rate of 70 cm^3 min^{-1}. Elemental composition and spatial distribution across the heterogeneous catalyst surface were determined through Energy Dispersive X-ray Spectroscopy (EDX) analysis, utilizing the mapping capabilities of the VEGA II Detector from TESCAN (Czech Republic). We meticulously examined the catalyst's surface morphology using the Field Emission Scanning Electron Microscopy (FESEM)/TE/SCAN instrument from Philips. To gain further insights into the catalyst's surface morphology, we conducted Transmission Electron Microscopy (TEM) analysis with the Philips TEM/CM 120 instrument. To explore the magnetic characteristics of the nanocatalyst in-depth, we employed a Vibrating Sample Magnetometry (VSM) instrument (model EZ-9) sourced from G. Colombo (Milano, Italy). This comprehensive array of state-of-the-art instruments ensured rigorous and thorough characterization of our catalyst materials and their inherent properties.

2.2. Typical procedure for the synthesis of the [Fe_3O_4@DAA-BTrzPhen–Cu(II)] composite

In the first step, Fe_3O_4 MNPs were prepared using a previously established procedure.[46] Simultaneously, 1 g of Fe_3O_4 MNPs were dispersed in a mixture of ethanol and water (1 : 1) (100 mL) for 45 min, and a 3 mmol of L-azidohomoalanine hydrochloride was added to the reaction mixture and then refluxed under vigorous stirring and a N_2 atmosphere for 3 days. Afterward, the resulting Fe_3O_4@L-AHA MNP product was magnetically collected, washed several times with ethanol and water and then dried under vacuum. Afterwards, 1.5 g of Fe_3O_4@L-AHA
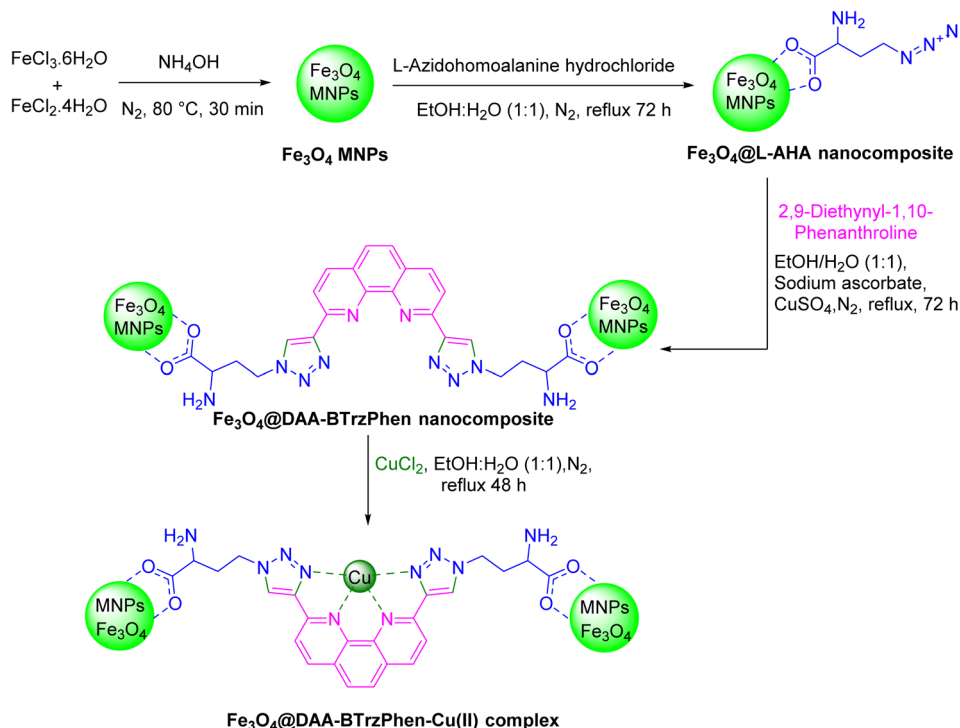
Scheme 1 Synthesis of the [Fe$_3$O$_4$@DAA-BTrzPhen–Cu(II)] composite.

and 1.5 mmol of 2,9-diethynyl-1,10-phenanthroline were dispersed in a mixture of ethanol and water (1 : 1) for 45 minutes. Then, 1 mL of an aqueous solution (2 M) of sodium ascorbate solution and 30 mg of copper sulfate pentahydrate in 10 mL of degassed water/DMSO 1 : 1 solvent mixture were added to the prepared suspension, respectively, and refluxed under vigorous stirring and a N$_2$ atmosphere for 3 days. Afterwards, the solid particles were collected magnetically, washed several times with ethanol and then with water and finally dried under vacuum. Finally, to a suspension of Fe$_3$O$_4$@DAA-BTrzPhen MNPs (1 g) in 100 mL of ethanol and water (1 : 1) was added 3 mmol CuCl$_2$·2H$_2$O and refluxed for 48 hours under vigorous stirring and a N$_2$ atmosphere. The obtained Fe$_3$O$_4$@DAA-BTrzPhen–Cu(II) composite was magnetically collected and washed successively with water and ethanol and dried under vacuum (Scheme 1).

2.3. General procedure to produce tetrasubstituted imidazoles over the catalysis of the [Fe$_3$O$_4$@DAA-BTrzPhen–Cu(II)] composite

In a round-bottomed flask, a mixture containing 1 mmol of aniline, 1 mmol of benzil, 1 mmol of aldehyde, and 12 mg of the [Fe$_3$O$_4$@DAA-BTrzPhen–Cu(II)] composite was prepared. To this mixture, 3 mL of ethanol was added, and the reaction was agitated under reflux conditions. The progress of the reaction was monitored using thin-layer chromatography (TLC). Once the reaction was deemed complete, a straightforward work-up procedure was conducted. The work-up procedure involved the evaporation of ethanol, followed by dilution with chloroform. The catalyst was then separated, and the organic layer was

washed successively with 3 × 5 mL of water, brine, and dried over anhydrous Na$_2$SO$_4$. The resulting solution was subsequently evaporated, yielding crude products. These crude products were purified using a column chromatographic technique with ethyl acetate and hexane as the eluent. Finally, the purified products were thoroughly characterized using ^{1}H and ^{13}C NMR spectroscopy (ESI†).

3. Results and discussion

3.1. Catalyst characterization

FT-IR analysis was conducted to evaluate the development of catalytic components on the surface. As depicted in Fig. 1, in the
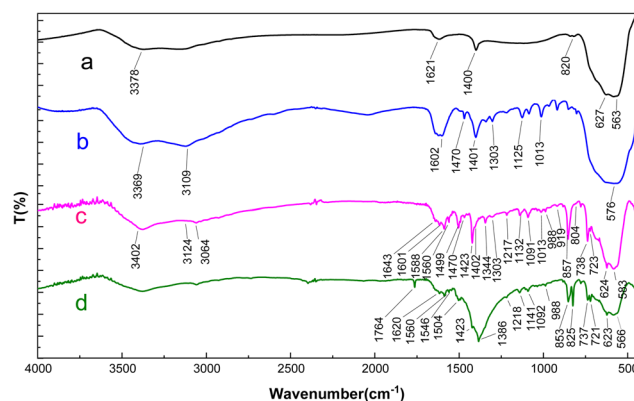
Fig. 1 FT-IR spectra of (a) Fe$_3$O$_4$ (b) Fe$_3$O$_4$@L-AHA (c) Fe$_3$O$_4$@DAA-BTrzPhen and (d) the [Fe$_3$O$_4$@DAA-BTrzPhen–Cu(II)] composite.

FT-IR spectra of Fe_3O_4 nanoparticles, the peaks detected at 563 cm^{-1} and 627 cm^{-1} indicate stretching vibrations within metal–oxygen bonds (as detailed in ref. 15). Furthermore, there is a broad peak in the 3100–3400 cm^{-1} range, which is attributed to O–H stretching vibrations.[47] In the FT-IR spectra of the Fe_3O_4@L-AHA nanocomposite, the broad absorption peak spanning from 2800–3500 cm^{-1} can be attributed to the presence of the carboxylic acid moiety of the L-azidohomoalanine linker beneath the surface, overlapping with aliphatic C–H and N–H stretching vibrations (related to methyl groups). The bands observed at 1470 cm^{-1}, 1401 cm^{-1}, 1302 cm^{-1}, 1125 cm^{-1}, and 1013 cm^{-1} indicate C–H stretching vibrations associated with aliphatic (methyl groups), carboxylic acid, C–N, and C–O bonds present within the L-AHA on the surface. Additionally, the successful synthesis of Fe_3O_4@DAA-BTrzPhen was confirmed by the emergence of characteristic peaks at 1402–1470 cm^{-1} (indicating the presence of C=C within the pyridine ring) and 1643 cm^{-1} (denoting C=N in the ligand). Moreover, the peaks in the 1200–1500 cm^{-1} range are related to C–N and C–O bonds. Furthermore, after the complexation of Cu with Fe_3O_4@DAA-BTrzPhen, the C=N bands shifted to lower frequencies, confirming the synthesis of the target complex.

X-ray diffraction (XRD) analysis, as shown in Fig. 2, was conducted to investigate the crystalline patterns of the Fe_3O_4 and [Fe_3O_4@DAA-BTrzPhen–Cu(II)] composite. The obtained XRD spectrum revealed distinct peaks at 30.15°, 35.70°, 43.3°, 57.45°, 54.25°, 62.90°, 71.43° and 74.29°, which can be attributed to the 220, 311, 222, 400, 422, 511, 440, 620 and 533 reflection planes, respectively.[48,49] The presence of these peaks provides compelling evidence for the existence of crystalline Fe_3O_4 magnetic nanoparticles (MNPs) within the complex. Consequently, it verifies the successful synthesis of Fe_3O_4 MNPs and confirms their structural stability even after the post-synthetic surface functionalization process. These findings validate the formation of the desired [Fe_3O_4@DAA-BTrzPhen–Cu(II)] composite and its potential applications in various fields such as catalysis. Calculating the size of nanoparticles using

Scherer's formula shows that the size of nanoparticles is about 17.44 nm.

The thermal stability and mass ratios of the [Fe_3O_4@DAA-BTrzPhen–Cu(II)] composite were assessed using TGA analysis (Fig. 3). Below 200 °C, there was an initial mass loss of around 5%, attributed to the evaporation of adsorbed moisture and solvents transforming into steam.[50] Subsequently, within the temperature range of 200–500 °C, the main mass loss of approximately 23% occurred due to the pyrolysis-driven disintegration of the organic components of the immobilized [DAA-BTrzPhen–Cu(II)] composite. These findings validate the successful functionalization of the Fe_3O_4 surface and the synthesis of the targeted nanocomposite. Importantly, the [Fe_3O_4@DAA-BTrzPhen–Cu(II)] composite demonstrated exceptional thermal stability, making it exceptionally well-suited for high-temperature catalytic applications. This exceptional thermal stability is a crucial characteristic that boosts its efficiency as a catalyst.
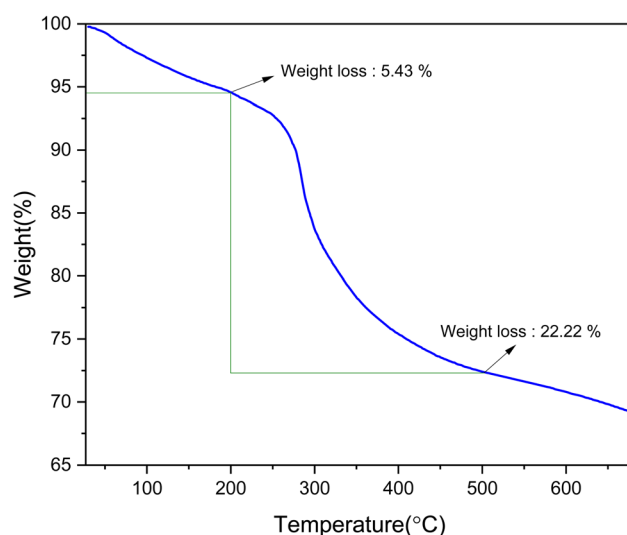
Fig. 3 TGA analysis of the [Fe_3O_4@DAA-BTrzPhen–Cu(II)] composite.
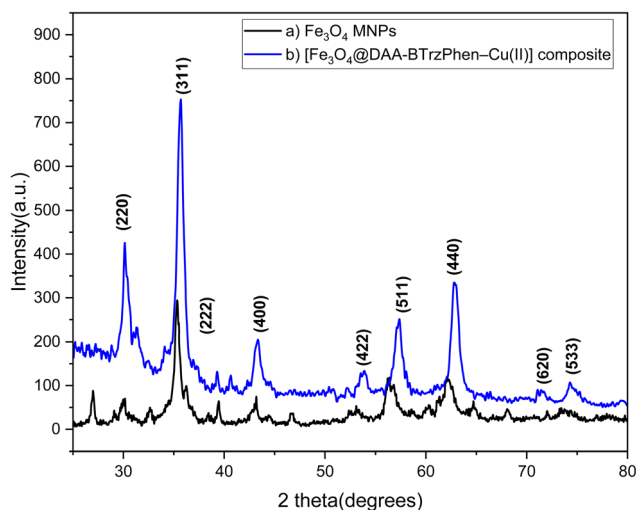
Fig. 2 XRD patterns of Fe_3O_4 and the [Fe_3O_4@DAA-BTrzPhen–Cu(II)] composite.
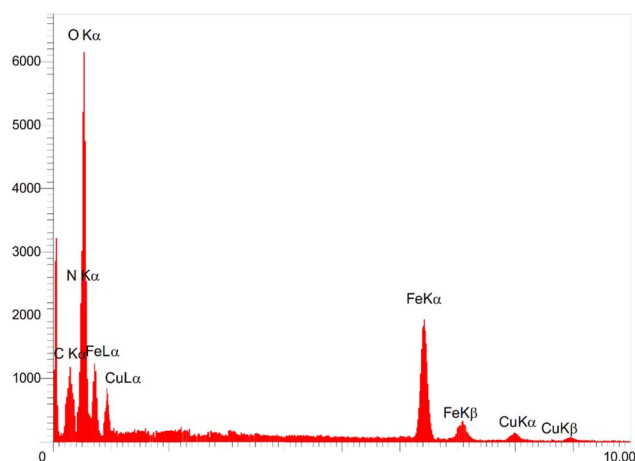
Fig. 4 EDAX analysis of the [Fe_3O_4@DAA-BTrzPhen–Cu(II)] composite.

The EDAX analysis (Fig. 4) was used to examine the elemental composition of the [Fe$_3$O$_4$@DAA-BTrzPhen–Cu(II)] composite. The results indicated the presence of inorganic Fe$_3$O$_4$ and copper ions, as evident from the appearance of Fe, O, and Cu peaks. These findings corroborated the TGA results, which demonstrated that over 70% of the sample consisted of inorganic materials, including the Fe$_3$O$_4$ support and copper. Furthermore, the identification of C and N peaks provided evidence of the successful functionalization of the Fe$_3$O$_4$ surface with the DAA-BTrzPhen ligand. To precisely determine the Cu content in the catalyst, ICP-OES analysis was conducted, yielding a Cu content of 1.37×10^{-5} mol g^{-1}. This analysis serves as confirmation of the successful synthesis of the targeted Cu complex.

The elemental mapping study, presented in Fig. 5, complements the EDX analysis by offering visual insights into the spatial distribution of elements within the [Fe$_3$O$_4$@DAA-BTrzPhen–Cu(II)] composite. The photographs show a high density of Fe and O elements and uniform distribution of C, N and Cu elemental components throughout the support material
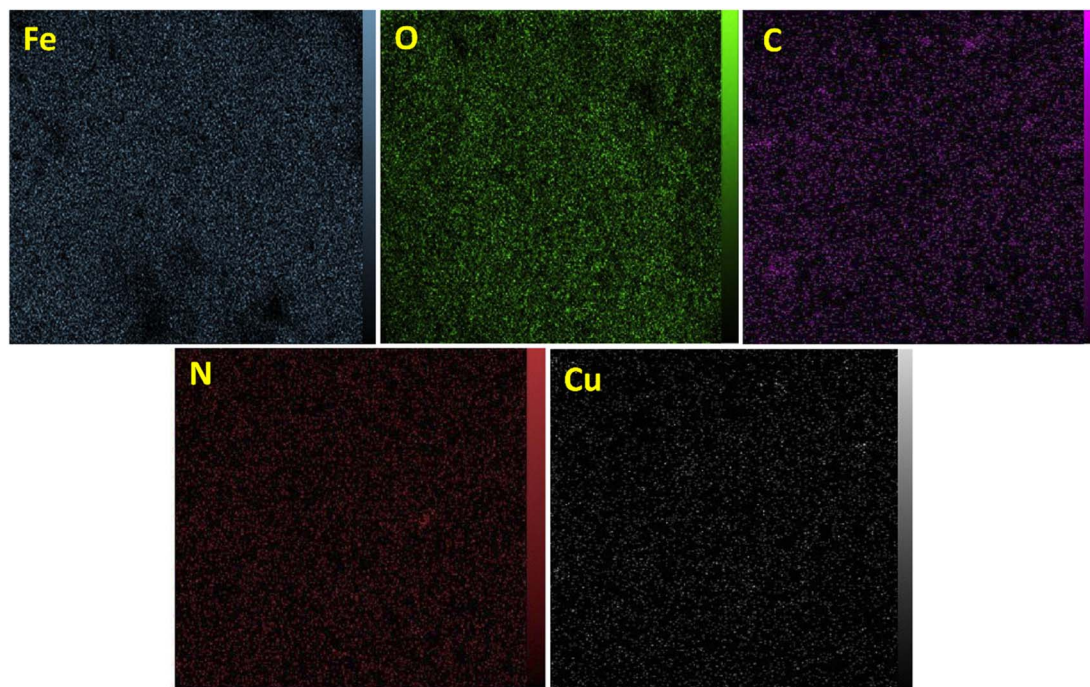
Fig. 5 Elemental mapping of the [Fe$_3$O$_4$@DAA-BTrzPhen–Cu(II)] composite.
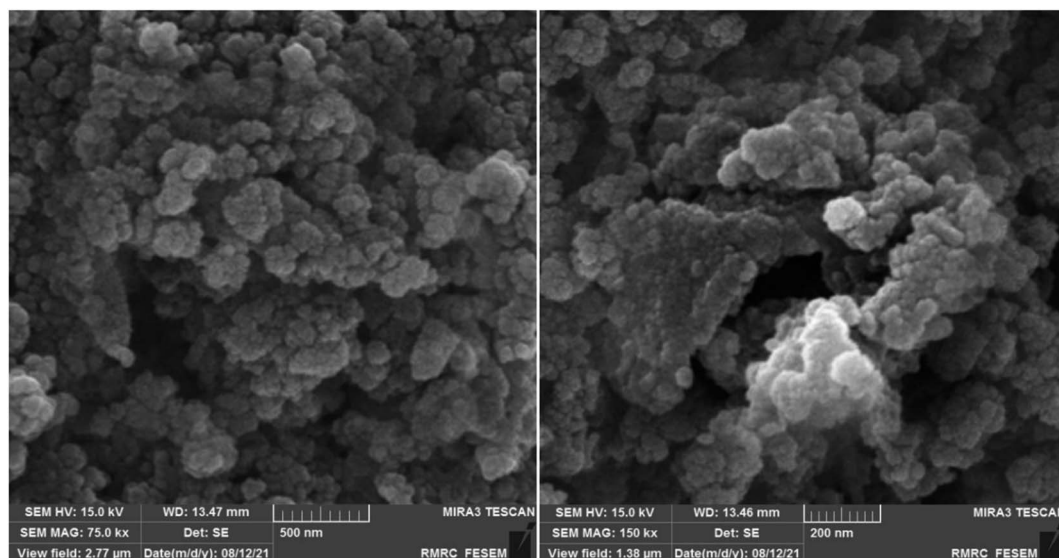
Fig. 6 SEM images of the [Fe$_3$O$_4$@DAA-BTrzPhen–Cu(II)] composite.
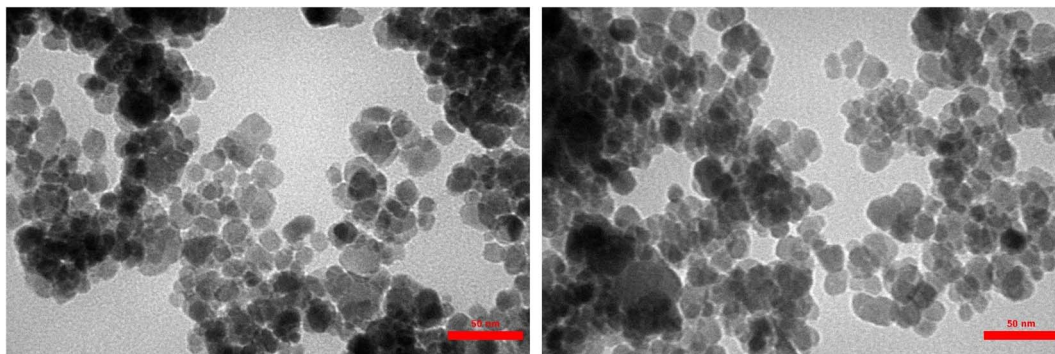
Fig. 7 TEM images of the [Fe$_3$O$_4$@DAA-BTrzPhen–Cu(II)] composite.
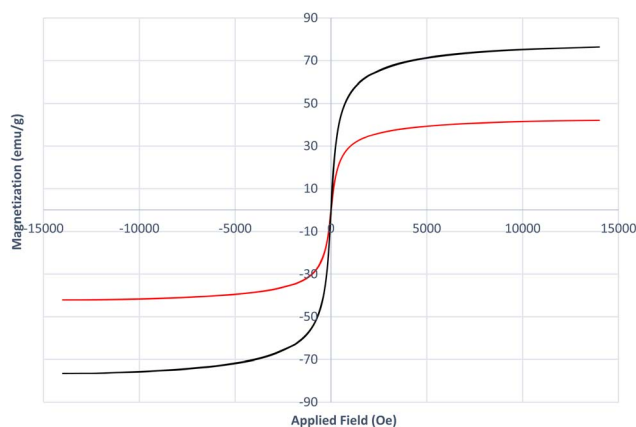
Fig. 8 VSM analysis of (a) Fe$_3$O$_4$ and (b) the [Fe$_3$O$_4$@DAA-BTrzPhen–Cu(II)] composite.

indicates a successful integration of the different catalyst moieties, suggesting a well-prepared and consistent structure.

Scanning Electron Microscopy (SEM) analysis was employed to meticulously investigate and elucidate the particle morphology and surface characteristics of the synthesized catalyst, as illustrated in Fig. 6. The meticulously crafted [Fe$_3$O$_4$@DAA-BTrzPhen–Cu(II)] composite exhibited a remarkable

and unmistakably spherical particle morphology. The surfaces of these particles were notably sleek and devoid of any discernible irregularities, portraying an exceptional degree of smoothness. Furthermore, the complex displayed an impressive level of uniformity in terms of particle size distribution, attesting to the precision of the synthesis process.

As demonstrated by TEM images (Fig. 7), the successful and precise deposition of the [DAA-BTrzPhen–Cu(II)] composite onto the surface of the Fe$_3$O$_4$ MNPs has been unmistakably unveiled. This coating manifests as a discernibly brighter periphery enveloping the darker core, imparting a well-defined spherical configuration. Notably, owing to the magnetic forces between the nanoparticles, a subtle assembly and stacking phenomenon becomes evident, as elegantly illustrated in Fig. 6. Delving deeper, the average particle size has been determined to fall within the range of approximately 17 nm to 25 nm, while retaining a predominantly spherical morphology. This exceptional uniformity in size underscores the precision inherent in the synthesis process.

VSM analysis (Fig. 8) was carried out to investigate the magnetic properties of both Fe$_3$O$_4$ and the [Fe$_3$O$_4$@DAA-BTrzPhen–Cu(II)] composite. The saturation magnetization value obtained for Fe$_3$O$_4$ was 76.4 emu g^{-1}, indicating its strong magnetic behavior. In contrast, the [Fe$_3$O$_4$@DAA-BTrzPhen–Cu(II)] composite displayed a lower magnetization value of 42
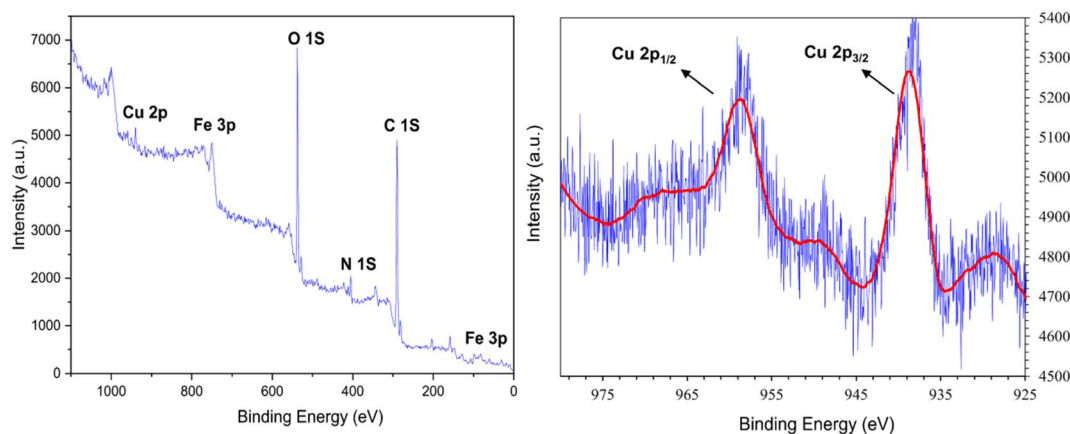
Fig. 9 XPS analysis of the [Fe$_3$O$_4$@DAA-BTrzPhen–Cu(II)] composite.

Adsorption / desorption isotherm
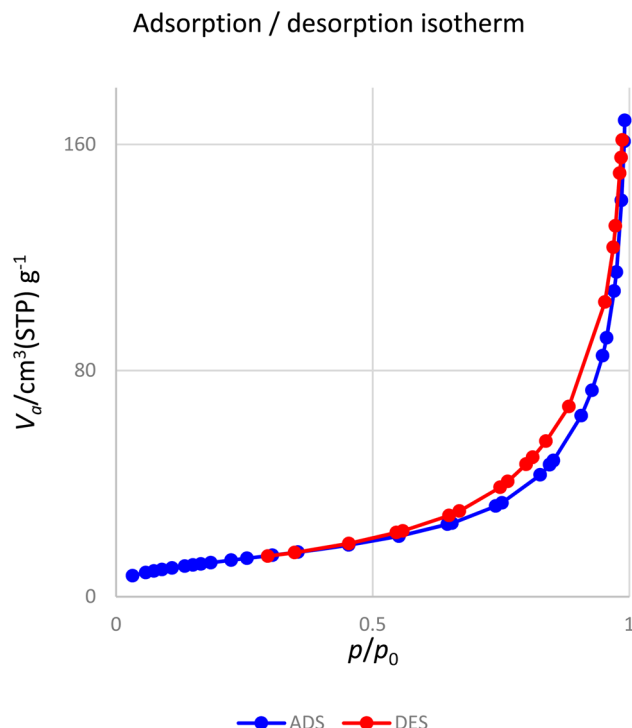
Fig. 10 N_2 adsorption–desorption analysis of the [Fe_3O_4@DAA-BTrzPhen–Cu(II)] composite.

emu g^{-1}, suggesting a reduction in magnetic response compared to pure Fe_3O_4 NPs. This reduction in magnetization can be attributed to the introduction of the ferromagnetic DAA-BTrzPhen ligand, which disturbs the uniformity of magnetic moments within the Fe_3O_4 NPs, leading to an overall decrease in magnetization. These findings validate the alteration of the nanocomposite's chemical composition and the successful synthesis of the targeted catalyst. Despite the decrease in magnetization after modification, the [Fe_3O_4@DAA-BTrzPhen–Cu(II)] composite still retains significant magnetic properties, rendering it a promising candidate for various applications in catalysis and environmental remediation.

The XPS analysis confirms the presence of expected peaks corresponding to Fe 2p, Fe 3p, C 1s, N 1s, O 1s, and Cu 2p within the [Fe_3O_4@DAA-BTrzPhen–Cu(II)] composite (Fig. 9). Notably, the observed bands include Fe–O (535.9 eV),[51] O–H (539.3 eV),[51] C–O (291.6 eV),[52] C–C (290.2 eV),[53] C–N (405.02 eV),[52] and C=N (405.23 eV),[52] aligning precisely with the composite's structural characteristics. Additionally, the XPS spectrum discloses two conspicuous peaks at approximately 938.15 eV and 948.73 eV, corresponding respectively to Cu $2p_{3/2}$ and Cu $2p_{1/2}$; this observation undeniably substantiates the presence of Cu species in the Cu(II) state within the prepared catalyst, in accordance with established literature.[52]

Fig. 10 presents the nitrogen adsorption–desorption isotherms of the [Fe_3O_4@DAA-BTrzPhen–Cu(II)] composite. The sample displays a characteristic type IV isotherm, conforming to the IUPAC's sorption isotherm classification. The nanoparticles possess a specific surface area of 74.9 m^2 g^{-1}, which plays a pivotal role in enhancing their catalytic efficiency.
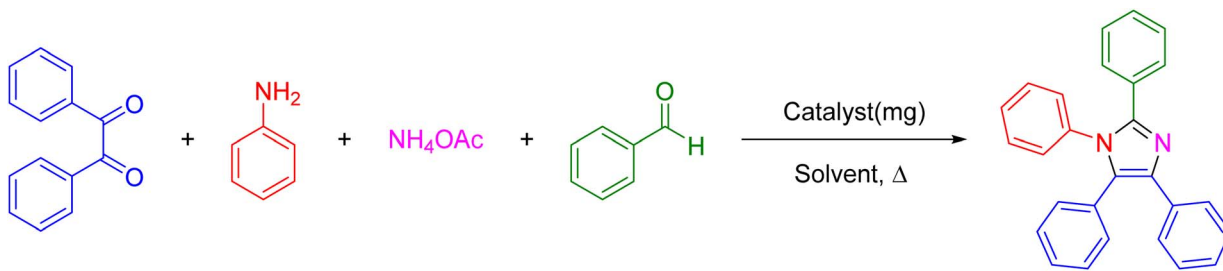
3.2. Catalytic study

To investigate the catalytic behavior of the [Fe_3O_4@DAA-BTrzPhen–Cu(II)] composite, we employed the cyclocondensation reaction of aniline, ammonium acetate and benzil with benzaldehyde as a model reaction. Various parameters were systematically examined to optimize the reaction conditions (Table 1). Initially, the reaction was conducted without any catalyst, but even after 8 hours, no product formation was observed (Table 1, entry 1). Next, we compared the catalytic performance of Fe_3O_4, Fe_3O_4@LAH, and Fe_3O_4@DAA-BTrzPhen intermediates with the [Fe_3O_4@DAA-BTrzPhen–Cu(II)] composite to assess the desired Cu complex (Table 1, entries 2–5). Among these, the [Fe_3O_4@DAA-BTrzPhen–Cu(II)] composite exhibited the most favorable results, leading to the highest product yield (Table 1, entry 5). In pursuit of enhanced conversion, we conducted additional investigations by varying the quantities of the [Fe_3O_4@DAA-BTrzPhen–Cu(II)] composite (Table 1, entries 5–9). Strikingly, the most remarkable efficiency was achieved when employing a 12 mg catalyst (Table 1, entry 8). This finding unequivocally highlights the significance of the catalyst's quantity in achieving optimal results.

In the quest for a suitable solvent, we evaluated a range of environmentally friendly options, such as ethanol, methanol, water, ethylene glycol, PEG-400, dimethylformamide, and solvent-free conditions (Table 1, entries 8, 10–15). After careful screening, ethanol emerged as the optimal choice and was selected as the primary solvent for the reaction (Table 1, entry 8). Its selection was based on its promising performance and compatibility with the optimal amount of the [Fe_3O_4@DAA-BTrzPhen–Cu(II)] composite. Next, different temperatures (Table 1, entries 2–6) were screened and it was observed that temperature influenced the product formation significantly, and the best conversion was obtained under reflux conditions. Finally, the optimal reaction conditions were determined with 12 mg of the [Fe_3O_4@DAA-BTrzPhen–Cu(II)] composite, in the presence of ethanol (3 mL) under reflux conditions (Table 1, entry 8).

In the subsequent step, we investigated the extensive applicability and adaptability of this method by utilizing the specified reaction conditions to analyze a diverse array of aniline and aldehyde substrates. This comprehensive set of aldehydes comprised various electron-donating and electron-withdrawing groups, such as halogens and naphthaldehyde functionalities. The experimental outcomes demonstrated remarkable yields of the desired tetrasubstituted imidazoles, underscoring the effectiveness of the approach (see Table 2). Interestingly, we observed that the electron-withdrawing groups significantly influenced both the reaction rate and yield, leading to the most favorable results. This discovery implies that electronic and hindrance effects play a critical role in the progression of the reaction. Furthermore, we successfully converted functionalized anilines into the target products, achieving impressive yields in remarkably short reaction times. This exceptional efficiency emphasizes the potential of this method for synthesizing tetrasubstituted imidazoles from a wide range of

Table 1 Optimization of the synthesis of tetrasubstituted imidazoles over the catalysis of the [Fe₃O₄@DAA-BTrzPhen–Cu(ɪɪ)] composite under different conditions

Entry	Catalyst	Amount of catalyst (mg)	Solvent	Temperature (°C)	Time (min)	Yield[a,b] (%)
1	—	—	EtOH	Reflux	480	NR
2	Fe₃O₄	5	EtOH	Reflux	15	Trace
3	Fe₃O₄@ʟ-AHA	5	EtOH	Reflux	15	27
4	Fe₃O₄@DAA-BTrzPhen	5	EtOH	Reflux	15	35
5	[Fe₃O₄@DAA-BTrzPhen–Cu(ɪɪ)]	5	EtOH	Reflux	15	71
6	[Fe₃O₄@DAA-BTrzPhen–Cu(ɪɪ)]	8	EtOH	Reflux	15	87
7	[Fe₃O₄@DAA-BTrzPhen–Cu(ɪɪ)]	10	EtOH	Reflux	15	95
8	[Fe₃O₄@DAA-BTrzPhen–Cu(ɪɪ)]	12	EtOH	Reflux	15	98
9	[Fe₃O₄@DAA-BTrzPhen–Cu(ɪɪ)]	15	EtOH	100	15	98
10	[Fe₃O₄@DAA-BTrzPhen–Cu(ɪɪ)]	12	MeOH	Reflux	15	96
11	[Fe₃O₄@DAA-BTrzPhen–Cu(ɪɪ)]	12	Water	Reflux	15	47
12	[Fe₃O₄@DAA-BTrzPhen–Cu(ɪɪ)]	12	Ethylene glycol	80	15	23
13	[Fe₃O₄@DAA-BTrzPhen–Cu(ɪɪ)]	12	PEG-400	80	15	29
14	[Fe₃O₄@DAA-BTrzPhen–Cu(ɪɪ)]	12	DMF	80	15	31
15	[Fe₃O₄@DAA-BTrzPhen–Cu(ɪɪ)]	12	DMSO	80	15	47
16	[Fe₃O₄@DAA-BTrzPhen–Cu(ɪɪ)]	12	Solvent-free	Reflux	15	84
17	[Fe₃O₄@DAA-BTrzPhen–Cu(ɪɪ)]	12	EtOH	60	15	87
18	[Fe₃O₄@DAA-BTrzPhen–Cu(ɪɪ)]	12	EtOH	40	15	58
19	[Fe₃O₄@DAA-BTrzPhen–Cu(ɪɪ)]	12	EtOH	r.t.	15	Trace

[a] Reaction conditions: benzil (1 mmol), aniline (1 mmol), benzaldehyde (1 mmol), ammonium acetate (1 mmol), catalyst (mg) and solvent (3 mL). [b] Isolated yields.

substrates, including those with intricate and heterocyclic structures.

The potential process for creating tetrasubstituted imidazole derivatives using the [Fe₃O₄@DAA-BTrzPhen–Cu(ɪɪ)] composite as a catalyst is depicted in Scheme 2. The initial step in this process involves a Schiff base reaction, in which the Cu-based composite acts as a Lewis acid. It engages with aldehyde carbonyl groups, activating them for nucleophilic attack by aryl amines. This interaction leads to the formation of the hemi-aminal intermediate (**I**), which subsequently undergoes the release of a water molecule to yield imine intermediate (**II**). In the following step, ammonia, produced from NH₄OAc, nucleo-philically attacks the imine intermediate, resulting in the formation of diamine intermediate (**III**). This intermediate then reacts with the activated benzil to yield (**IV**). The elimination of a water molecule leads to the formation of intermediate (**V**). The subsequent step involves an intramolecular nucleophilic attack by the amine group on the activated carbon. This is followed by a process to remove water from intermediate (**VI**) and produc-tion of the final products and the release of the nanocatalyst.

3.3. Reusability tests

One of the most captivating benefits demonstrated by hetero-geneous nanocatalysts pertains to their exceptional recover-ability and potential for reuse. To further substantiate this recyclability, a series of examinations were carried out on the [Fe₃O₄@DAA-BTrzPhen–Cu(ɪɪ)] nanocatalyst, focusing specifi-cally on its role in the synthesis of tetrasubstituted imidazoles through the cyclocondensation reaction involving aniline, ammonium acetate and benzil, where benzaldehyde served as the representative reaction model. Following the reaction completion, the nanocatalyst was effortlessly separated from the reaction mixture using an external magnet. Subsequent purification with ethyl acetate and acetone, coupled with a drying procedure, readied the nanocatalyst for subsequent usage. Remarkably, the [Fe₃O₄@DAA-BTrzPhen–Cu(ɪɪ)] nano-catalyst consistently displayed recyclability across eight cycles, maintaining a substantial yield as visually depicted in Fig. 11. Following eight cycles, the recovered [Fe₃O₄@DAA-BTrzPhen–Cu(ɪɪ)] nanocatalyst was evaluated using FT-IR and BET analyses (Fig. 12 and 13). The composition of functional groups and

Table 2 The synthesis of tetrasubstituted imidazole derivatives over the catalysis of the [Fe₃O₄@DAA-BTrzPhen–Cu(II)] composite in ethanol
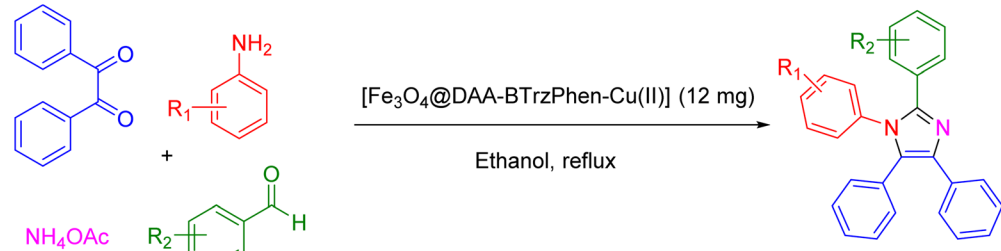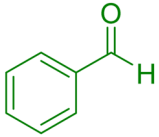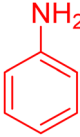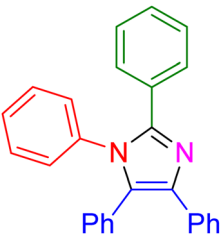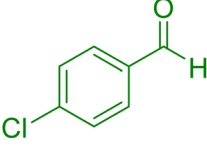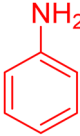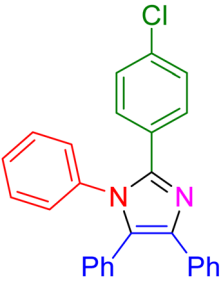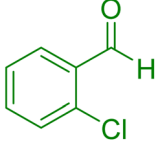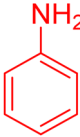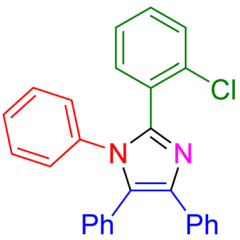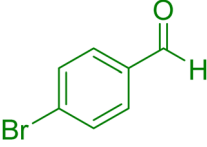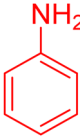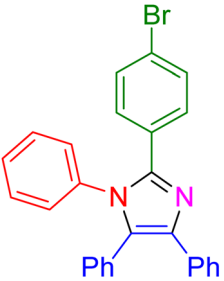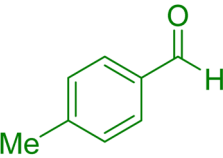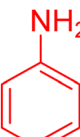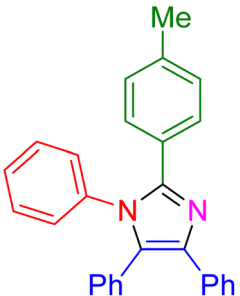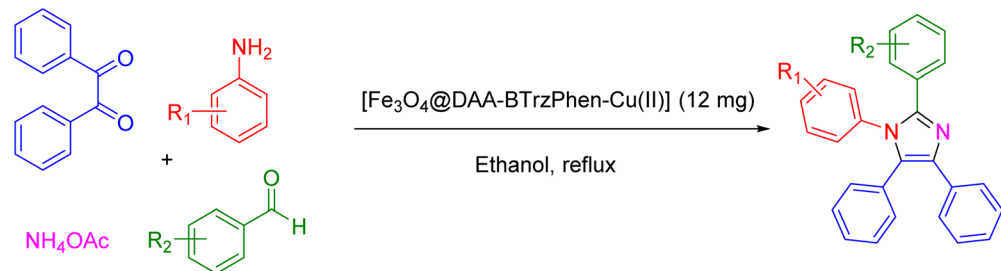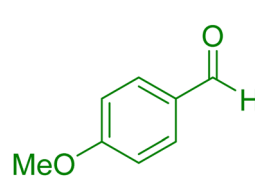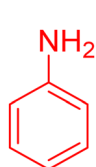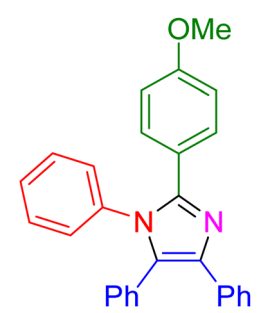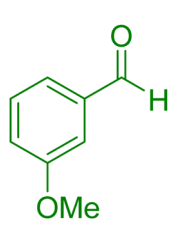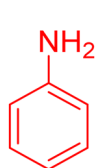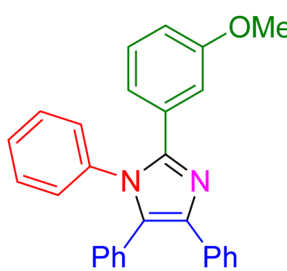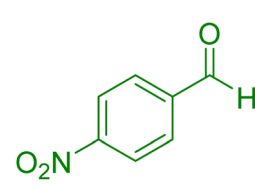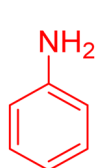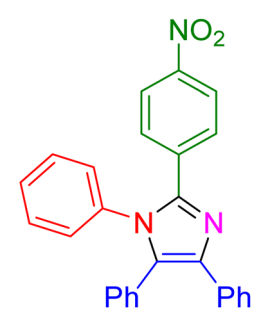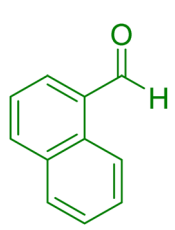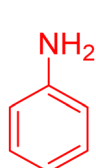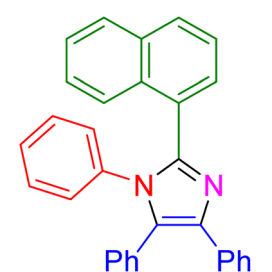
Entry	Aldehyde	Aniline	Product	Time (min)	Yield[a,b] (%)
1				15	98
2				17	96
3				20	93
4				15	95
5				15	97

Table 2 (*Contd.*)

Entry	Aldehyde	Aniline	Product	Time (min)	Yield^{a,b} (%)
6				25	93
7				25	95
8				10	98
9				25	92

Table 2 (Contd.)
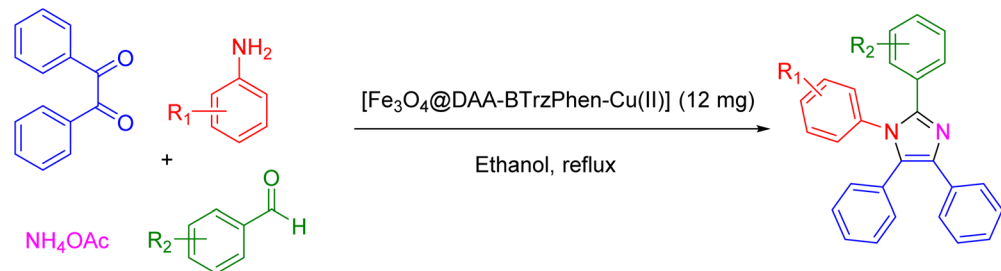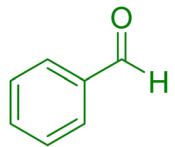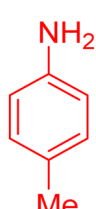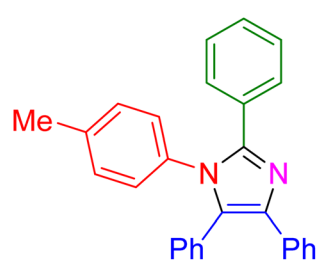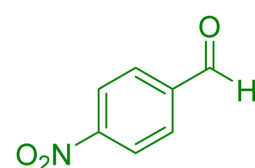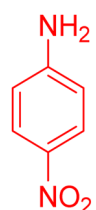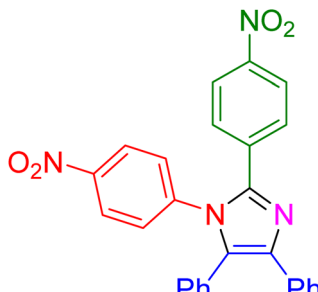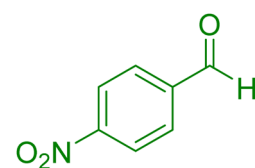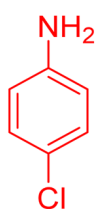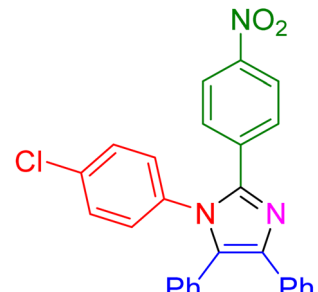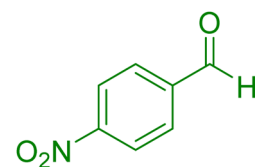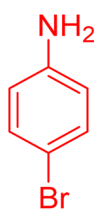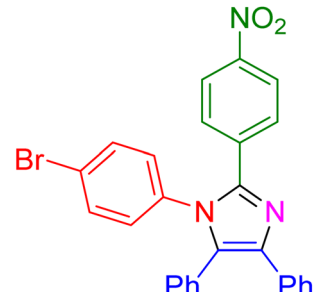
Entry	Aldehyde	Aniline	Product	Time (min)	Yield^{a,b} (%)
10	(benzaldehyde)	(4-methylaniline)	(2-phenyl-1-(4-methylphenyl)-4,5-diphenylimidazole)	15	97
11	(4-nitrobenzaldehyde)	(4-nitroaniline)	(2-(4-nitrophenyl)-1-(4-nitrophenyl)-4,5-diphenylimidazole)	30	96
12	(4-nitrobenzaldehyde)	(4-chloroaniline)	(2-(4-nitrophenyl)-1-(4-chlorophenyl)-4,5-diphenylimidazole)	17	97
13	(4-nitrobenzaldehyde)	(4-bromoaniline)	(2-(4-nitrophenyl)-1-(4-bromophenyl)-4,5-diphenylimidazole)	15	98
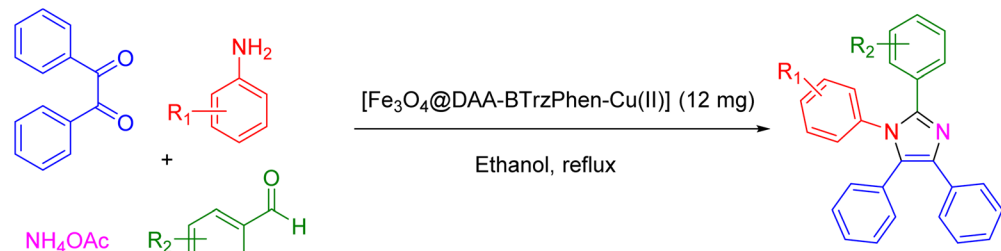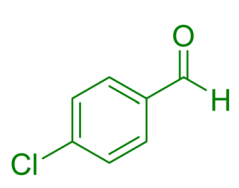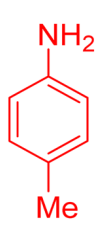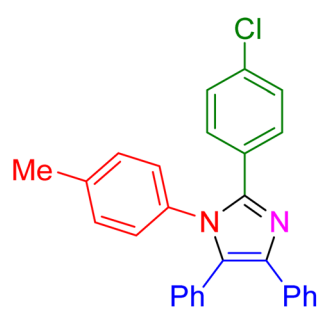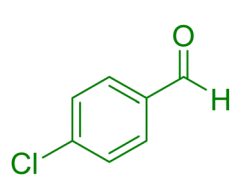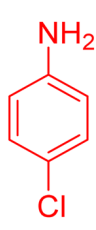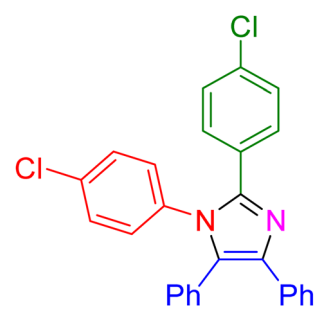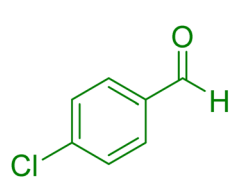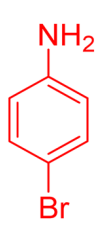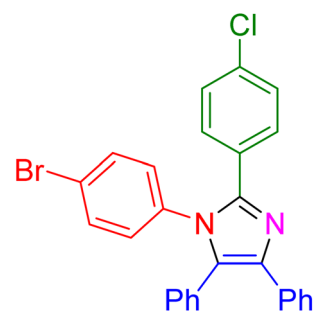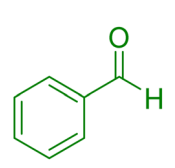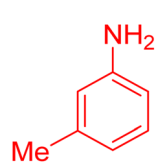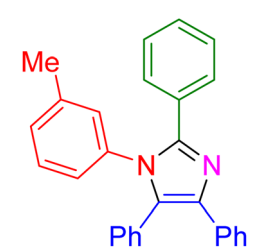
Table 2 (*Contd.*)

Entry	Aldehyde	Aniline	Product	Time (min)	Yield^{a,b} (%)
14				20	96
15				27	95
16				25	95
17				18	96

Table 2 (*Contd.*)
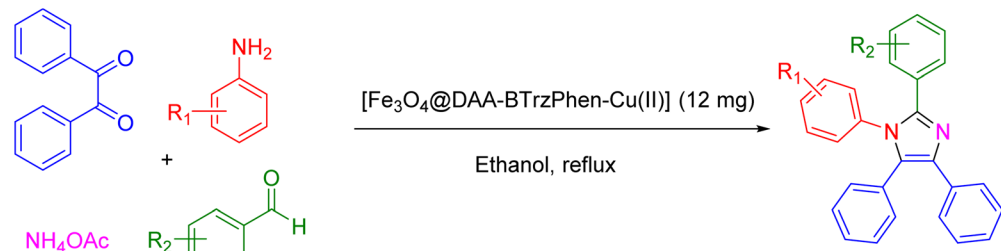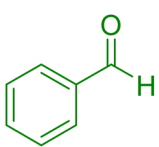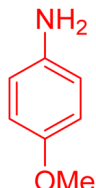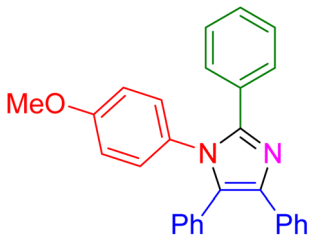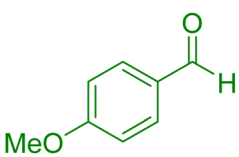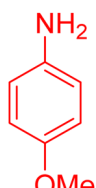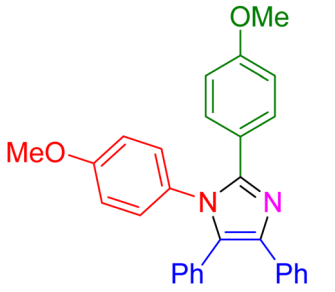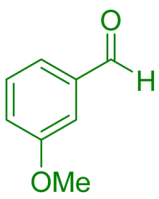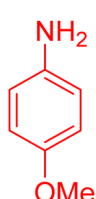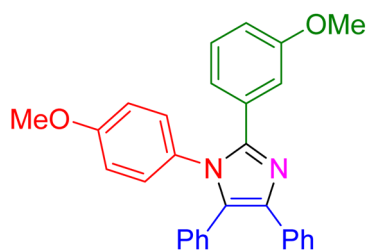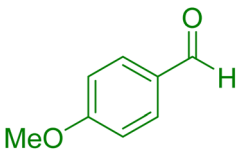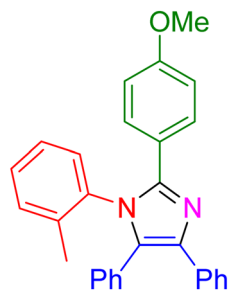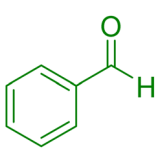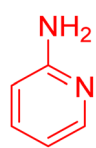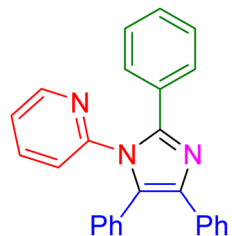
Entry	Aldehyde	Aniline	Product	Time (min)	Yield[a,b] (%)
18	benzaldehyde	4-methoxyaniline	product	10	98
19	4-methoxybenzaldehyde	4-methoxyaniline	product	20	95
20	3-methoxybenzaldehyde	4-methoxyaniline	product	30	95
21	4-methoxybenzaldehyde	2-methylaniline	product	30	93
22	benzaldehyde	2-aminopyridine	product	20	97

Table 2 (*Contd.*)

Entry	Aldehyde	Aniline	Product	Time (min)	Yield^{a,b} (%)
23				20	96

^{a} Conditions: benzil (1 mmol), aniline (1 mmol), aldehyde (1 mmol), ammonium acetate (1 mmol) and [Fe$_3$O$_4$@DAA-BTrzPhen–Cu(II)] (12 mg) under reflux of ethanol (3 mL). ^{b} Isolated yields.
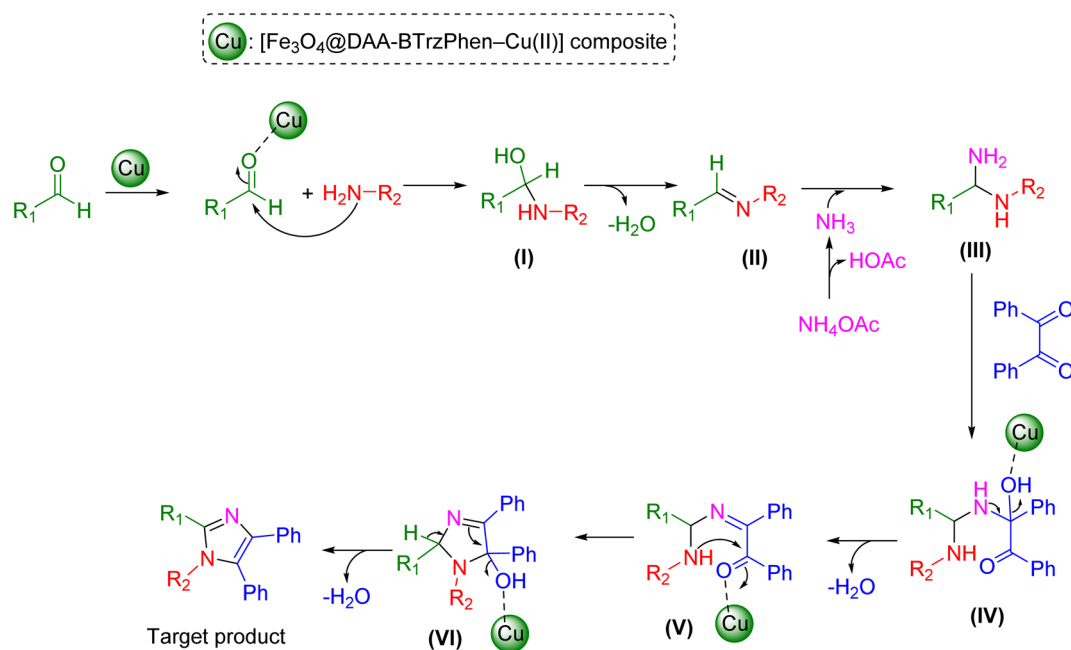
Scheme 2 Possible mechanism for the synthesis of tetrasubstituted imidazole derivatives over the catalysis of the [Fe$_3$O$_4$@DAA-BTrzPhen–Cu(II)] composite.

surface properties observed in the used catalyst closely mirror those of the pristine catalyst. This observation substantiates the enduring stability of the catalytic components attached to the Fe$_3$O$_4$ support during the reaction and recycling process.

3.4. Hot-filtration and leaching tests

To evaluate the potential for copper leaching from the nanocatalyst, a hot-filtration test was conducted on the model reaction. The nanocatalyst was employed until achieving a 74%
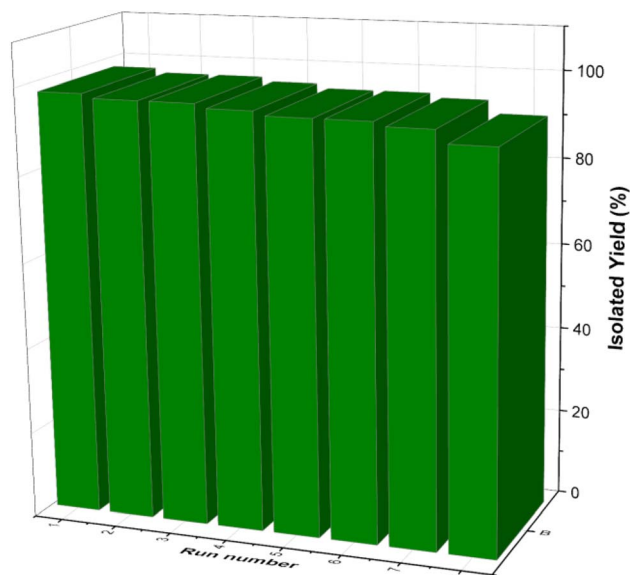
Fig. 11 Reusability of the [Fe$_3$O$_4$@DAA-BTrzPhen–Cu(II)] composite.
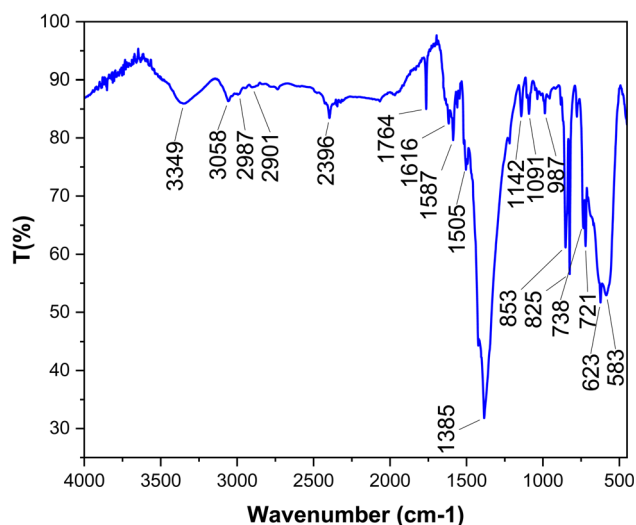
Fig. 12 FT-IR spectra of the recycled [Fe$_3$O$_4$@DAA-BTrzPhen–Cu(II)] composite.

conversion rate (after 30 minutes). At this point, magnetic separation facilitated the catalyst extraction from the heated reaction mixture. The reaction mixture was subsequently transferred to another container, permitting the reaction to proceed for an additional 30 minutes, followed by an evaluation of the reaction yield. Notably, no further conversion was discerned, signifying an absence of notable growth in product formation.

Further analysis encompassing inductively coupled plasma atomic emission spectroscopy (ICP-OES) was executed on the filtrate. The results from this analysis demonstrated that the copper content in the filtrate was negligible. This outcome provided compelling evidence affirming that the catalytic process was unequivocally driven by heterogeneity, with minimal to no observable instances of copper leaching.
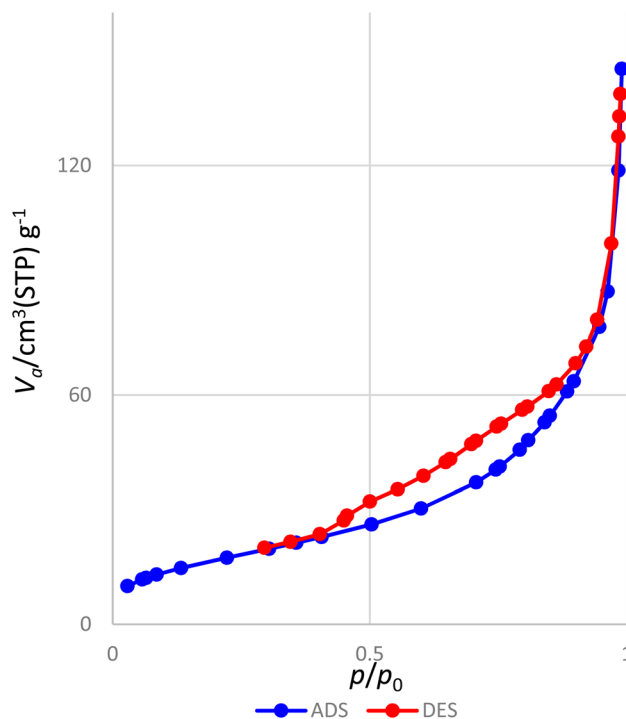

Fig. 13 N$_2$ adsorption–desorption analysis of the recovered [Fe$_3$-O$_4$@DAA-BTrzPhen–Cu(II)] composite.

Table 3 Comparison of the catalytic efficiency of the [Fe$_3$O$_4$@DAA-BTrzPhen–Cu(II)] composite in the synthesis of tetrasubstituted imidazoles using the condensation of aniline, ammonium acetate, benzil and benzaldehyde

Entry	Catalyst	Time (min)	Yield[a] (%)	References
1	HNa$_2$[PMo$_{12}$O$_{40}$]	120	88	54
2	1-Methyl-3-(4-sulfobutyl) imidazolium	150	88	55
3	PWA/SiO	17	70	56
4	γ-Alumina	10	85	57
5	[Fe$_3$O$_4$@DAA-BTrzPhen–Cu(II)]	15	98	This work

[a] Isolated yield.

3.5. Comparison

To evaluate the excellence of our current study relative to previously recorded techniques, we performed a comparative assessment between the performance of the developed nano-catalyst in synthesizing tetrasubstituted imidazoles and that of preceding catalysts. The outcomes of this comparison have been succinctly outlined in Table 3. Our approach showcased several noteworthy benefits, including a straightforward experimental process, favorable reaction conditions, reduced catalyst demand, and a noteworthy yield of the targeted product.

4. Conclusions

In this study, we have introduced an innovative nanomagnetic Cu complex, anchored by a synthetic bistriazolylphenanthroline ligand attached to the Fe_3O_4 surface, showcasing its prowess as a highly effective heterogeneous catalyst. This catalyst has demonstrated its potential in facilitating the synthesis of diverse pharmaceutically significant tetrasubstituted imidazoles through a streamlined one-pot multicomponent condensation process, involving anilines, ammonium acetate, 1,2-diketones, and aldehydes. This methodology not only prioritizes environmental friendliness and straightforward purification procedures but also operates under mild reaction conditions, reducing reaction time, and yielding remarkable product quantities. Additionally, the catalyst's convenient retrieval using a magnet further enhances its practicality. This heterogeneous nanocatalyst holds great promise in the realm of synthesizing related heterocyclic compounds through multicomponent reactions, a potential attributed to its unique features, notably the abundance of reactive catalytic species integrated into its structure.

Conflicts of interest

There are no conflicts to declare.

Acknowledgements

References

1 R. Sahoo, S. Mondal, S. Chand and M. C. Das, *Inorg. Chem.*, 2023, **62**(32), 12989–13000.

2 N. Moeini-Eghbali and H. Eshghi, *Inorg. Chem. Commun.*, 2023, **156**, 111181.

3 X. Yang, H. Duan, R. Wang, F. Zhao, F. Jin, W. Jiang, G. Han, Q. Guan and H. Ben, *Inorg. Chem.*, 2023, **62**(33), 13419–13427.

4 A. N. Bilyachenko, I. S. Arteev, V. N. Khrustalev, L. S. Shul'pina, A. A. Korlyukov, N. S. Ikonnikov, E. S. Shubina, Y. N. Kozlov, N. Reis Conceição, M. F. C. Guedes da Silva, K. T. Mahmudov and A. J. L. Pombeiro, *Inorg. Chem.*, 2023, **62**(33), 13573–13586.

5 R. Lima Oliveira, K. A. Ledwa, O. Chernyayeva, S. Praetz, C. Schlesiger and L. Kepinski, *Inorg. Chem.*, 2023, **62**(33), 13554–13565.

6 F. Ghobakhloo, D. Azarifar, M. Mohammadi, H. Keypour and H. Zeynali, *Inorg. Chem.*, 2022, **61**, 4825–4841.

7 S. G. Krishnan, F.-L. Pua and F. Zhang, *Biomass Bioenergy*, 2021, **149**, 106099.

8 E. Karakhanov, A. Maximov and A. Zolotukhina, *Polymers*, 2022, **14**, 981.

9 M. Gholinejad, F. Zareh, H. Sheibani, C. Nájera and M. Yus, *J. Mol. Liq.*, 2022, **367**, 120395.

10 J. Tang, X. Liu, S. Cao, S. Zhang, H. Zhang, L. Zhu, J. Ji and J. Wang, *J. Phys. Chem. C*, 2021, **125**, 23736–23743.

11 S. H. Gebre, *Appl. Nanosci.*, 2023, **13**(1), 15–63.

12 M. E. Aldokheily, A. H. Mekky and S. A. Rahem, *Chem. Methodol.*, 2022, **6**, 494–500.

13 S. Ghorbani, D. Habibi, S. Heydari, M. Mohammadi and M. Ariannezhad, *Environ. Sci. Pollut. Res.*, 2022, **30**, 32762–32775.

14 A. Dehno Khalaji, P. Machek and M. Jarosova, *Adv. J. Chem., Sect. A*, 2021, **4**, 317–326.

15 F. Ghobakhloo, D. Azarifar, M. Mohammadi and M. Ghaemi, *Appl. Organomet. Chem.*, 2022, **36**, e6823.

16 Y. Chen, Z. Chen and J. Wei, *ACS Appl. Nano Mater.*, 2023, **6**(16), 14702–14709.

17 M. O. Azeez, S. A. Nafiu, T. A. Olarewaju, A. B. Olabintan, A. Tanimu, Y. Gambo and A. Aitani, *Ind. Eng. Chem. Res.*, 2023, **62**(33), 12795–12828.

18 X.-Y. Wei, X. Bai, F.-Y. Ma, Z.-M. Zong, W. Zhao, Z.-H. Ni, X. Fan, L.-B. Sun, J.-P. Cao, Y.-P. Zhao, S.-C. Qi, J. Liang, X.-M. Yue, F.-J. Liu, W.-L. Mo, J.-M. Liu, Y.-H. Kang, G.-H. Liu, Z.-Q. Liu and L. Li, *Energy Fuels*, 2023, **37**(17), 12570–12588.

19 L. Rubab, A. Anum, S. A. Al-Hussain, A. Irfan, S. Ahmad, S. Ullah, A. A. Al-Mutairi and M. E. A. Zaki, *Catalysts*, 2022, **12**(11), 1329.

20 A. R. Liandi, A. H. Cahyana, A. J. F. Kusumah, A. Lupitasari, D. N. Alfariza, R. Nuraini, R. W. Sari and F. C. Kusumasari, *Case Stud. Chem. Environ. Eng.*, 2023, **7**, 100303.

21 F. Zhu and P. Yin, *J. Org. Chem.*, 2023, **88**, 4352–4358.

22 I. Lee, K. Bang, H. Yang and T. Choi, *Macromol. Rapid Commun.*, 2022, **43**, 2100642.

23 S. Sen, D. Barman, H. Khan, R. Das and D. Maiti, *J. Org. Chem.*, 2022, **87**, 12164–12174.

24 G. Pawar, S. M. Ghouse, S. V. Joshi, P. Rana, S. Kar, P. M. Sarma, S. R. Dannarm, R. Sonti and S. Nanduri, *ChemistrySelect*, 2022, 7(14), e20220050.

25 R. Zhang, Y. Chen, M. Ding and J. Zhao, *Nano Res.*, 2022, **15**, 2810–2833.

26 R. Singh, G. G. Singh, N. George, G. G. Singh, S. Gupta, H. Singh, G. Kaur and J. Singh, *Catalysts*, 2023, **13**, 130.

27 A. I. B. Romo, M. P. dos Reis, O. R. Nascimento, P. V. Bernhardt, J. Rodríguez-López and I. C. N. Diógenes, *Coord. Chem. Rev.*, 2023, **477**, 214943.

28 M. M. Matin, P. Matin, M. R. Rahman, T. Ben Hadda, F. A. Almalki, S. Mahmud, M. M. Ghoneim, M. Alruwaily and S. Alshehri, *Front. Mol. Biosci.*, 2022, **9**, 864286.

29 S. H. Sumrra, W. Zafar, M. Imran and Z. H. Chohan, *J. Coord. Chem.*, 2022, **75**, 293–334.

30 A. Fauzi, A. Saifudin and K. Rullah, *J. Med. Chem. Sci.*, 2023, **6**, 1810–1817.

31 M. kidwai, P. Dwivedi and A. Jahan, *J. Appl. Organomet. Chem.*, 2023, **3**, 156–168.

32 V. Estévez, M. Villacampa and J. C. Menéndez, *Chem. Soc. Rev.*, 2010, **39**, 4402.

33 R. M. Mhaibes, Z. Arzehgar, M. M. Heydari and L. Fatolahi, *Asian J. Green Chem.*, 2023, 7, 1–8.

34 R. Muslim Muhiebes, L. Fatolahi and S. Sajjadifar, *Asian J. Green Chem.*, 2023, 7, 121–131.

35 M. A. Bodaghifard, M. Hamidinasab and N. Ahadi, *Curr. Org. Chem.*, 2018, 22, 234–267.

36 Y. Wang, A. A. Cobo and A. K. Franz, *Org. Chem. Front.*, 2021, 8, 4315–4348.

37 A. Takeda, H. Okai, K. Watabe and H. Iida, *J. Org. Chem.*, 2022, 87, 10372–10376.

38 F. Xu, W.-J. Zhu, P.-W. Wang, J. Feng, X.-R. Chen, X.-H. Han and H.-T. Yan, *J. Org. Chem.*, 2023, 88, 9811–9822.

39 H. M. Pineda-Castañeda, Z. J. Rivera-Monroy and M. Maldonado, *ACS Omega*, 2023, 8, 3650–3666.

40 R. Li, F. Zhou, X. Huang, J. Zhao and H. Zhang, *J. Org. Chem.*, 2023, 88, 739–744.

41 D. A. Shabalin and J. E. Camp, *Org. Biomol. Chem.*, 2020, 18, 3950–3964.

42 D. G. Daraji, N. P. Prajapati and H. D. Patel, *J. Heterocycl. Chem.*, 2019, 56, 2299–2317.

43 N. Kerru, S. V. H. S. Bhaskaruni, L. Gummidi, S. N. Maddila, S. Maddila and S. B. Jonnalagadda, *Synth. Commun.*, 2019, 49, 2437–2459.

44 A. Mishra, J. Aslam, C. Verma, M. A. Quraishi and E. E. Ebenso, *J. Taiwan Inst. Chem. Eng.*, 2020, 114, 341–358.

45 P. Sharma, C. LaRosa, J. Antwi, R. Govindarajan and K. A. Werbovetz, *Molecules*, 2021, 26, 4213.

46 M. Kazemnejadi, S. A. Alavi G, Z. Rezazadeh, M. A. Nasseri, A. Allahresani and M. Esmaeilpour, *Appl. Organomet. Chem.*, 2020, 34, e5388.

47 H. Eslahi, A. Reza Sardarian and M. Esmaeilpour, *ChemistrySelect*, 2021, 6, 1984–1993.

48 E. Bertolucci, A. M. R. Galletti, C. Antonetti, M. Marracci, B. Tellini, F. Piccinelli and C. Visone, in *2015 IEEE International Instrumentation and Measurement Technology Conference (I2MTC) Proceedings*, IEEE, 2015, pp. 1492–1496.

49 S. Molaei, M. Ghadermazi and N. Moeini, *Appl. Surf. Sci. Adv.*, 2022, 7, 100192.

50 F. Ashouri, A. R. Faraji, Z. Hekmatian and A. Farahanipour, *Chem. Pap.*, 2022, 76, 3581–3605.

51 X. Tang, Q. Feng, K. Liu, Z. Li and H. Wang, *J. Mater. Sci.*, 2018, 53, 369–384.

52 H. Ebrahimiasl and D. Azarifar, *Appl. Organomet. Chem.*, 2020, 34(3), e5359.

53 A. H. Kianfar and M. A. Arayesh, *J. Environ. Chem. Eng.*, 2020, 8, 103640.

54 M. M. Heravi, F. Derikvand and F. F. Bamoharram, *J. Mol. Catal. A: Chem.*, 2007, 263, 112–114.

55 A. Davoodnia, M. M. Heravi, Z. Safavi-Rad and N. Tavakoli-Hoseini, *Synth. Commun.*, 2010, 40, 2588–2597.

56 E. Rafiee, H. Mahdavi and M. Joshaghani, *Mol. Diversity*, 2011, 15, 125–134.

57 P. Shelke, A. Rajbhoj, M. Nimase, G. Tikone, B. Zaware and S. Jadhav, *Orient. J. Chem.*, 2016, 32, 2007–2014.